JOURNAL OF SPACECRAFT AND ROCKETS
Vol. 29, No. 5, September–October 1992

Characterization of Advanced Flexible Thermal Protection Material for Space Applications

Joseph P. Clayton*
Remtech, Inc., Huntsville, Alabama 35805
and
Michael L. Tinker†
NASA Marshall Space Flight Center, Huntsville, Alabama 35812

This paper describes experimental and analytical characterization of a new flexible thermal protection material known as Tailorable Advanced Blanket Insulation (TABI). This material utilizes a three-dimensional ceramic fabric core structure and an insulation filler. TABI is the leading candidate for use in deployable aeroassisted vehicle designs. Such designs require extensive structural modeling, and the most significant in-plane material properties necessary for model development are measured and analytically verified in this study. First, nonlinear modulus curves are presented for the directions parallel and normal to the fill direction. Trends observed in the modulus profiles are explained in terms of filament behavior. Next, the dominant damping type and approximate magnitudes are determined using log decrement and hysteresis methods. Because of the clothlike nature of the material, unusual test methods are used for damping measurements. Mathematical models are developed for verification of the experimental modulus and damping data, and finally, transverse properties are described in terms of the in-plane properties through use of a finite difference model of a simple TABI configuration.

Introduction

FUTURE space applications of ceramic fabric materials will require extensive structural modeling of the fabrics. The clothlike nature of these materials complicates measurement of mechanical properties required for modeling. Properties readily available for metallic or composite rigid materials are not available for fabrics. This is not surprising, since fabrics historically have not been used as structural members. Fabric manufacturers have not felt the need to provide structural properties. Filament and yarn data, which are normally provided by manufacturers, are not indicative of overall fabric properties and should not be used for two reasons. First, the modulus, strength, and damping properties of fabrics are governed in part by the degree of slip motion between yarns and filaments. Filament data do not account for these slippage effects. Second, fiber contact stresses and residual stresses resulting from the weaving process weaken the fabric compared to an individual filament.

Use of advanced fabrics for structural applications is obviously difficult due to the high flexibility of the materials and the lack of mechanical property data, as discussed in the previous paragraph. However, ceramic fabrics have great potential for use in spacecraft thermal protection systems due to their ability to withstand the high temperatures encountered in the space environment.[1-8] One application of a fabric thermal protection system (TPS) being considered for future space missions is the deployable aerobrake (Fig. 1). An aerobrake is a blunt structure on the front of a spacecraft that would allow the use of aerodynamic drag to provide vehicle deceleration for orbital transfers. The deceleration would occur during a controlled trajectory (aeropass) of the vehicle through a planetary atmosphere.[9]

A new ceramic TPS, called Tailorable Advanced Blanket Insulation (TABI), has been developed by NASA Ames Research Center for applications such as aerobraking.[1,2] Past research has resulted in an incomplete data base of TABI structural properties, including density, fabric tensile strength, and filament elastic modulus. For analytical modeling of TABI and an aerobrake structure incorporating it, the overall material modulus of elasticity and damping characteristics (type and magnitude) are required. The purpose of this investigation is to experimentally obtain the needed TABI structural properties and to verify them in analytical models.

Description of Tailorable Advanced Blanket Insulation

TABI consists of two parallel sheets of ceramic fabric connected by triangular or rectangular cores, as shown in Fig. 2.

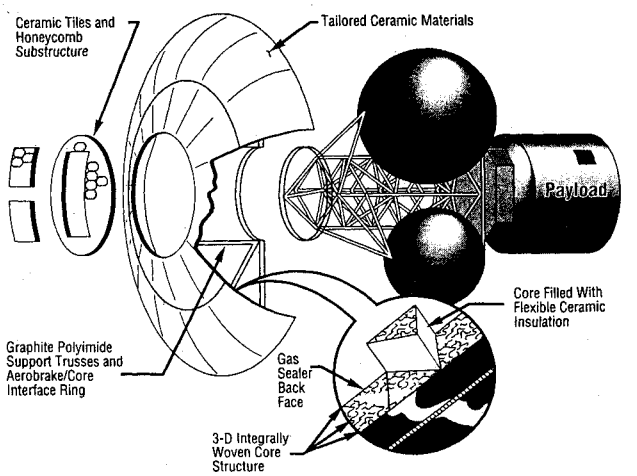

Fig. 1 Deployable aerobrake concept utilizing tailorable advance blanket insulation.

Received March 7, 1991; presented as Paper 91-1047 at the AIAA/ASME/ASCE/AHS/ASC 32nd Structures, Structural Dynamics, and Materials Conference, Baltimore, MD, April 8-10, 1991; revision received Dec. 29, 1991; accepted for publication Jan. 15, 1992.

*Senior Engineer.
†Aerospace Technologist, Systems Research Branch. Member AIAA.

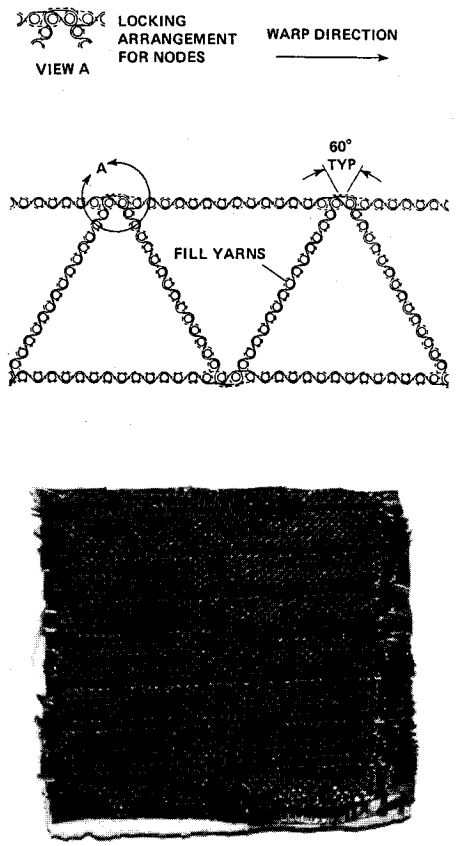

Fig. 2 Cross-sectional side view and top view of TABI sample.

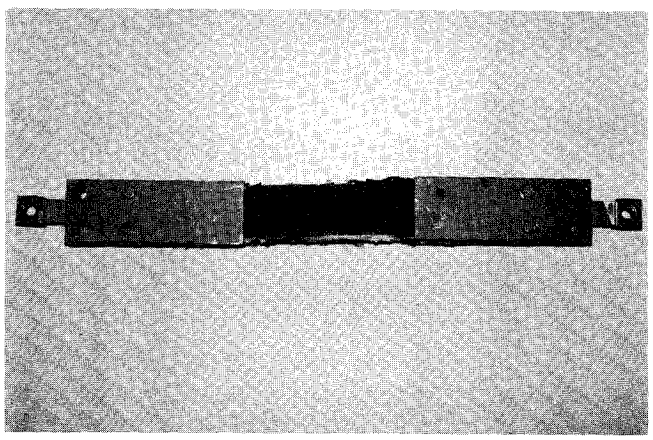

Fig. 3 Material specimen used for elastic modulus tests.

The cores extend along the entire length of the fabric sheets and are filled with fibrous ceramic insulation. The material has greater strength in the direction parallel to the cores (fill direction) than in the direction normal to the cores (warp direction). Currently, silicon carbide fibers are used to weave the fabric, and silica is used as the filler insulation material. Alumina is also being considered as a possible insulation material and may be substituted for the silica due to its superior thermal properties.

Sections of TABI are joined using two different mechanisms. One mechanism, called a tadpole joint, is used to orient the joint parallel to the warp direction. The second mechanism orients the joint parallel to the fill direction. Both joints are constructed of tubular silicon carbide yarn filled with silica batting. Reference 1 contains further information on the structure of TABI and the joining mechanisms.

Experimental Characterization of Tailorable Advanced Blanket Insulation In-Plane Stiffness and Damping Properties

Modulus Testing

The success of math modeling techniques for flexible fabrics or any material is obviously dependent on the material data available. Most significant among the material properties that characterize TABI is the elastic modulus. As stated in Ref. 10, use of manufacturer's filament modulus data for an entire fabric yields inaccurate results. Therefore, a test program was designed to estimate the overall material modulus of elasticity.

Modulus tests were performed using an Instron testing machine with a loading frame. TABI specimens were cut from a large sample of material in strips 2.0 in. wide and 0.75 in. thick, as shown in Fig. 3. The aluminum fixtures in Fig. 3 were constructed to grip the ends of the specimens and provide attachment points for the loading frame. As described in Ref. 11, seven modulus tests were performed, including fill and warp direction testing. Of those seven sets of data, two fill direction curves were averaged and used along with the best warp direction curve to obtain approximate modulus curves. All tests were performed at room temperature, and the specimens were loaded to failure to allow measurement of break strength in addition to the elastic moduli.

Figure 4 shows the general profile of the experimental stress-strain curves. It can be seen that the modulus is nonlinear, increasing as the strain increases. Stiffening results from tightening of the fibers as strain increases. For small loads and deflections, considerable mechanical slippage occurs between fiber bundles, but for larger loads, the fabric tightens and restricts this motion. Therefore, the initial portion of the curve in Fig. 4 is dominated by mechanical slippage, whereas the remainder of the curve is likely associated with a combination of fiber bundle slippage and filament elongation.

As stated previously, the test articles were loaded to failure to determine the break strength and observe the nature of the failure. Figure 4 shows that failure of the TABI material occurs as a propagation of filament breakages rather than a sudden failure of the entire sample. Some filaments fail before others because of nonuniform loading, variable diameters of filaments, and the inability to produce a completely homogeneous weave in the fabrication process.

Modulus values were calculated from experimental stiffness curves using the assumption that TABI is a homogeneous material 0.75 in. thick and 2.0 in. wide. If this assumption were not made, the cross-sectional areas of all of the filaments would have to be added statistically, thus complicating the reduction and use of the data. In Eqs. (1) and (2), the moduli for the fill and warp directions are expressed as continuous functions of strain,

Fill:

$$m(\epsilon) = 1{,}845{,}200(\epsilon)^{1.147} \tag{1}$$

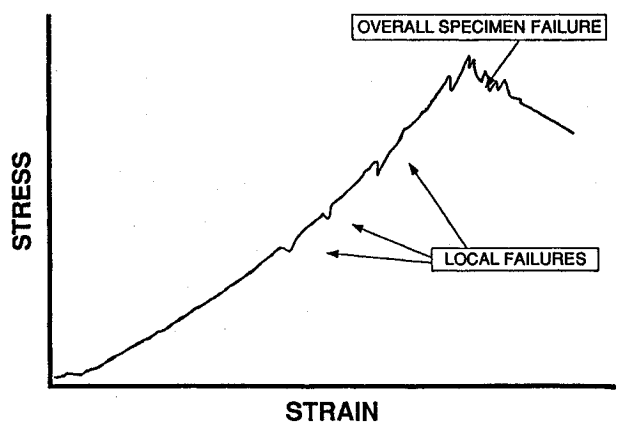

Fig. 4 Profile of experimental stress-strain curves.

Warp:

$$m(\epsilon) = 144{,}744(\epsilon)^{0.634} \quad (2)$$

and in Figs. 5 and 6, the corresponding experimental stress-strain curves are shown in piecewise linear form. As stated previously, the fill direction modulus curve represents the average of two sets of test data, and the warp direction curve was obtained from the best data available. The average maximum break strength for the fill direction is 665 lb, and the warp direction break strength is 195 lb.

A much more detailed discussion of the test procedures and data analysis is given in Ref. 11. Modulus and break strength values presented in this paper should be considered specific to the TABI material used for the tests. The material tested was associated with a certain weave; it was constructed of silicon carbide filaments whose diameters can only be determined statistically, and each specimen had some variation in loading due to variations in the material/fixture bonded surface (Fig. 3). All of these parameters have some variation from one material sample to another, and although the properties presented in this paper are representative for TABI in general, they should be considered approximate.

It is noted here that the modulus curves are very similar to those for rubber structures.[12,13] More will be said later about similarities between TABI and viscoelastic materials. Finally, the filler insulation is not considered to add strength or stiffness, but it contributes mass and affects the damping properties of the material.

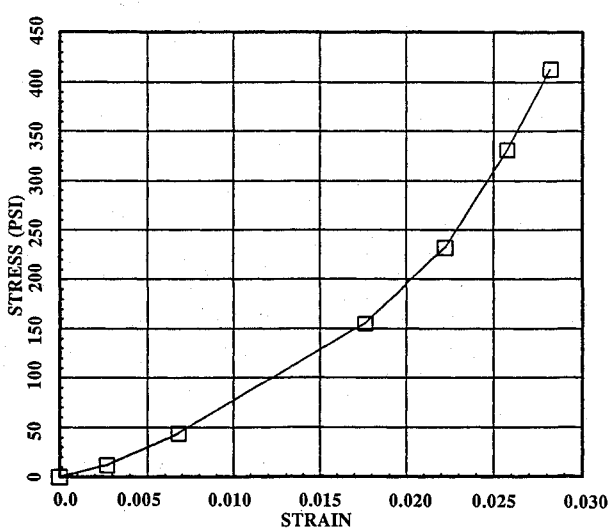

Fig. 5 TABI elastic modulus curve for fill direction.

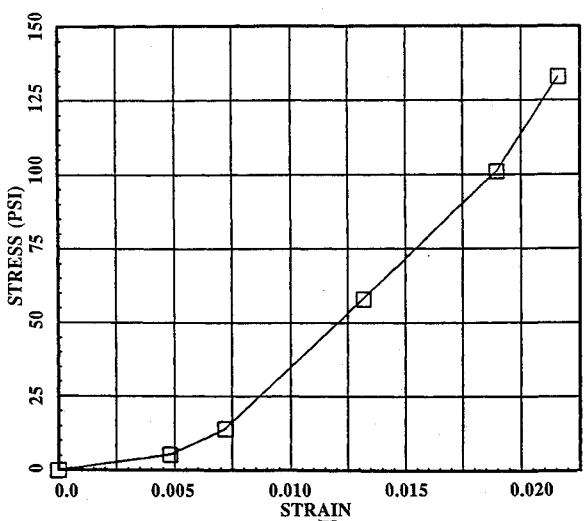

Fig. 6 Elastic modulus curve for warp direction.

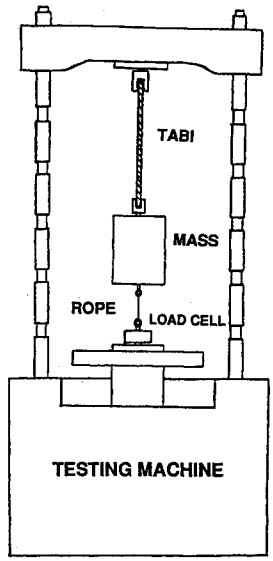

Fig. 7 Arrangement for log decrement damping tests.

Damping Tests

Determination of damping properties is critical to dynamic characterization of deployable aerobrake designs that utilize TABI as a thermal protection system. For many structures, damping forces are very small and do not play an extremely critical role. However, due to the structure of TABI, in which individual fibers have considerable freedom to slide relative to each other, damping forces are of greater importance in deployable aerobrake structures. Damping could be of sufficient degree to significantly affect modal survey tests and make dynamic testing difficult in general. Modal testing could be affected for two main reasons. First, damping can prevent uniform distribution of excitation energy in a large test article, making modal identification difficult or impossible. Second, heavy damping can cause coupling of modes in large flexible meshlike structures such as aerobrakes so that recognizable mode shapes cannot be observed.[14]

Severe damping can present even greater problems for the analyst. Adequate analytical representation of damping forces requires proper definition of the type and magnitude of damping in the math model. If nonproportional damping is required in the model, the dynamic system matrices are asymmetric and the eigenvalues are complex. The greater the degree of damping in the structure, the more important it becomes to understand the damping mechanism. For these reasons, several tests were planned to aid in identifying the type and degree of damping present in the TABI material.

Damping experiments have been performed for both free and forced vibration of TABI specimens similar to those described in the previous section. The samples were 2.0 in. wide and 0.5 in. thick with a length of 7.0 in. Test articles were preloaded with a series of masses to assure that the material remained in tension throughout the tests. Tensile preloading is necessary for damping tests of flexible fabrics since in-plane compression loads cannot be sustained.

Logarithmic Decrement Testing

For free-vibration damping tests, the TABI/mass system was arranged with the upper edge of the specimen fixed to a support (Fig. 7). A load cell was used at the mass-loaded end of the specimen to apply additional tensile load to the material. The additional load was released suddenly, and the free response of the mass was measured using an accelerometer. In Fig. 8 a typical acceleration time history is shown, in which the

free oscillation occurs at approximately 30 Hz. Additional data and a detailed discussion of the damping test procedures are given in Ref. 11.

Damping coefficients for the TABI/mass system were calculated using the logarithmic decrement method, and it was found that the average damping is approximately 6% of critical. It is noted here that a TPS constructed of TABI is expected to be much more heavily damped than the simple system described earlier. This issue will be discussed further in the next section.

It is seen from Fig. 8 that the vibration amplitude decays in a nearly exponential manner. This observation provides a first indication that viscous damping may be representative of the in-plane dissipative forces in the material.[15] The free-vibration response can also be used in another manner to estimate the type of damping present in TABI. It is realized that multiple damping mechanisms are present in most structural systems. However, the dominant mechanism can be estimated from semilog plots of maximum amplitude vs number of cycles of free oscillation.[16] As shown in Fig. 9 (reproduced from Ref. 16), if the damping is viscous, or hysteretic with the energy dissipated per cycle proportional to the square of the amplitude, the semilog plot is linear. The slope of the line is the logarithmic decrement. For hysteretic damping with the dissipated energy proportional to the amplitude raised to a power greater than two, the plot is concave upward. If dry friction is present, the curve is concave downward.

Semilog plots of amplitude vs number of cycles for two free-vibration tests are shown in Fig. 10. The plots appear to indicate that all three damping mechanisms discussed earlier are present in TABI, but they also show some variation in damping characteristics between material samples. The lower curve in Fig. 10 indicates the presence of dry friction for higher amplitudes. It was expected before the experiments that dry friction would be observed due to the slip motion between fibers. Although clear identification of the type of damping cannot be made from Fig. 10, it can be seen that the semilog plot profile does not deviate drastically from a straight line (viscous damping), especially for small amplitudes. To further aid in identifying the damping mechanism and the degree of damping, a series of forced-vibration tests was planned. These experiments are described in the next section.

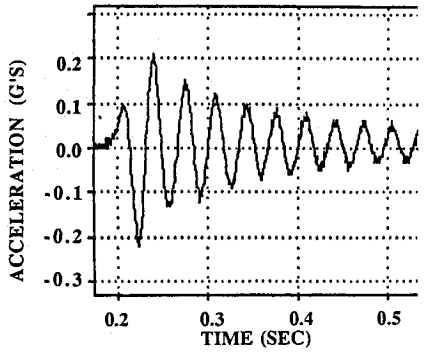

Fig. 8 Acceleration time history for log decrement test.

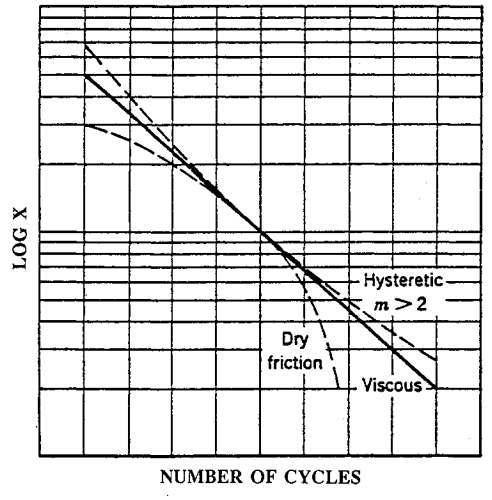

Fig. 9 Damping type as function of semilog plot profile (Ref. 16, copyright © 1989 by John Wiley and Sons, Inc. Reprinted by permission).

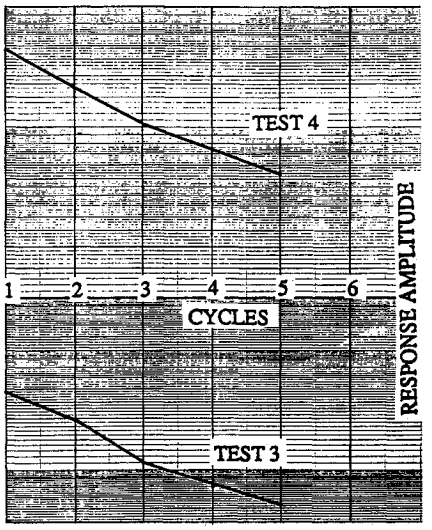

Fig. 10 Semilog profiles for free-vibration damping tests.

Hysteresis Curve Measurements

For systems with substantial dissipation of energy, hysteresis curves are perhaps the most important indicator of the type and magnitude of damping. The area enclosed by a hysteresis loop gives the energy dissipated per cycle, and the shape of the loop is determined by the damping type.[17] Several tests have been performed using mass-preloaded TABI specimens and an electrodynamic shaker to obtain the force-displacement hysteresis curves. As stated previously, unusual test techniques are required for flexible fabrics since the test articles must be maintained in tension. The test configuration is shown in Fig. 11. Experiments were conducted for several frequencies from approximately 20–50 Hz, for three amplitudes below 0.003 in., and for three mass preloads from 50–175 lb. The masses chosen envelope the expected loads for a deployable aerobrake in an aeropass maneuver.

Representative hysteresis curves for the 75-lb preload are shown in Figs. 12 and 13 for two excitation frequencies. The force plotted in Figs. 12 and 13 is that transmitted to the upper fixture, and the displacement is that of the mass. The amplitudes of excitation are indicated by arrows for each curve. The most important observation to be made is that the curves are nearly elliptical in shape, although nonlinear stiffness is apparent for the highest amplitude 41-Hz case shown in Fig. 13. This observation provides further evidence that viscous damping is present in the TABI material for low amplitudes of excitation. It is expected that in-plane oscillations of TABI will be of low amplitude in the aerobraking environment. Therefore, these findings and the results of the free-vibration tests indicate that viscous damping may provide an adequate model of TABI in-plane damping.

Several other interesting observations can be made from the experimental hysteresis curves in Figs. 12 and 13. First, the damping energy consistently increases for increased excitation amplitude, possibly due to increased slippage between fibers in the test articles. In agreement with this observation, Ref. 13

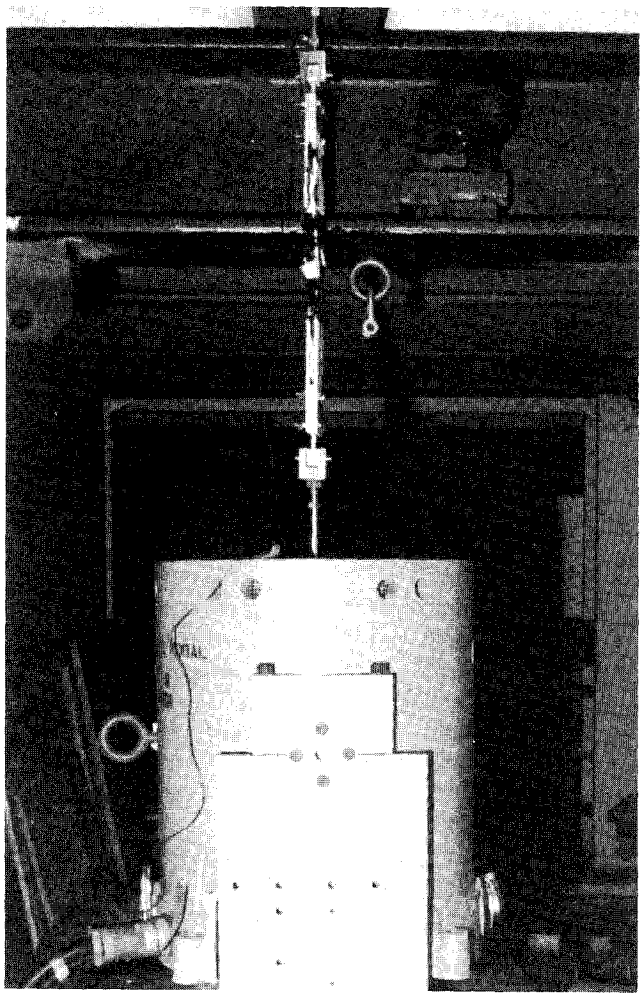

Fig. 11 Test configuration for measurement of hysteresis curves.

states that the effects of nonlinearity usually result in higher levels of damping for increased excitation amplitude. Second, the damping energy varies with frequency in a complicated manner. For the 75-lb preload, it was found that the damping increases to a peak near 26 Hz and decreases for higher frequencies. This behavior indicates that TABI has properties similar to those observed for many viscoelastic materials.[13] Third, for each frequency, the stiffness consistently decreases as amplitude increases. Similar behavior is observed for rubber vibration isolators containing carbon and for wire rope structures.[18] Since TABI fibers are formed from a carbon compound, the stiffness variation with amplitude appears reasonable in terms of both microscopic material behavior and

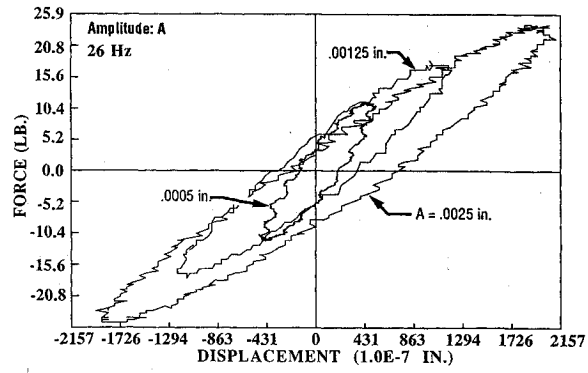

Fig. 12 Experimental hysteresis curves, 26 Hz.

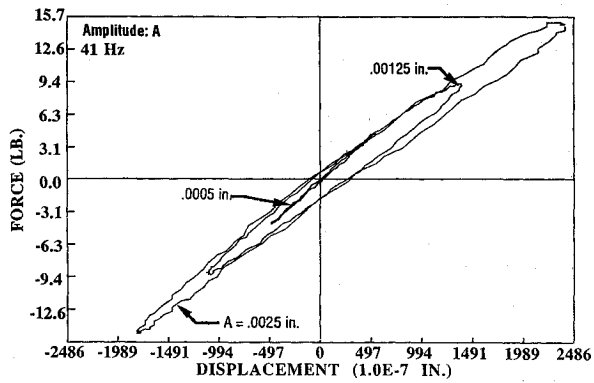

Fig. 13 Experimental hysteresis curves, 41 Hz.

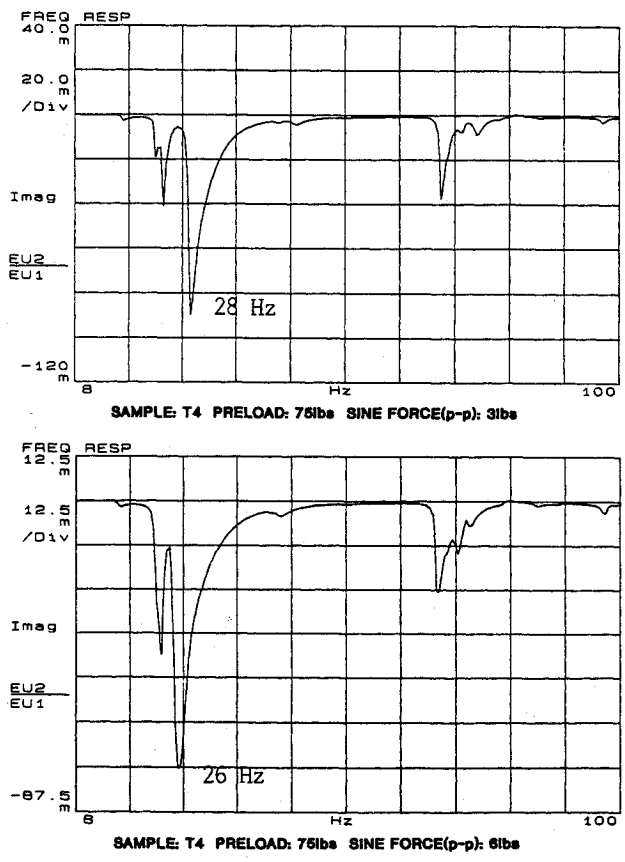

Fig. 14 Experimental frequency responses of TABI/mass system.

higher level fiber interaction. The important conclusion to be made from these observations is that TABI properties appear to be as readily explained in terms of viscoelastic material behavior as in terms of fiber slippage or friction.

The decrease in stiffness for increased amplitude can also be seen from the frequency response functions in Fig. 14. As the driving force is increased from 3 to 6 lb, the resonant frequency of the TABI/mass system shifts downward from approximately 28 to 26 Hz. Shifts in the resonant frequency were observed throughout the test data, illustrating the highly nonlinear character of TABI.

Changes in preload have a very interesting effect on the damping characteristics of the material. It has been observed that, for both the 50- and 175-lb mass loads, the material has low damping compared to the 75-lb case. One explanation for this behavior is that the 50-lb load does not tighten the material enough to cause significant sliding friction between the fibers, whereas the 175-lb load causes the material to be so taut that the fibers have little freedom to slide and dissipate energy. The TABI load levels are not well identified for the aerobraking environment, but the results for the 50- and 75-lb cases are considered representative. However, regardless of the magnitude of damping, it appears that, for low excitation amplitudes, viscous damping can provide an adequate representation of the type of TABI in-plane energy dissipation.

For comparison to the logarithmic decrement tests, damping coefficients have been calculated using the basic expressions

$$c = W_D/(\pi\Omega Z^2) \tag{3}$$

$$c_{cr} = 2k/\omega_n = 2\sqrt{km} \tag{4}$$

where W_D is the area enclosed by a hysteresis curve; Ω and Z are the frequency and amplitude of excitation, respectively; and ω_n is the system natural frequency. The average of the damping ratios c/c_{cr} for the TABI/mass system was found to be approximately 0.06 for the 75-lb preload, comparing well with the logarithmic decrement results. For the 50-lb preload, the average damping was approximately 2% of critical.

As discussed in the section describing free-vibration tests, a TPS constructed of TABI is expected to be much more heavily damped than the simple TABI/mass system. Using the mass of the material samples alone (0.037 lb) in Eq. (4) for c_{cr}, along with the viscous damping coefficients calculated previously from Eq. (3), the average damping ratio c/c_{cr} for TABI alone was found to be approximately 3.74 using the stiffness associated with a 75-lb preload. This rough calculation shows that the material is heavily overdamped. Such severe damping is expected to make future modal tests of an aerobrake article very difficult. On the other hand, damping of this magnitude should suppress structural vibration of the aerobrake in an aeropass maneuver, making instabilities such as flutter unlikely.

Mathematical Models of Damping Test Configurations

In order to verify test results for TABI stiffness and damping properties and to initiate development of modeling techniques, several mathematical models have been studied. In this section, two of those models are discussed. First, a model representing the logarithmic decrement test and using a restoring force expression derived from stiffness test data is described. Then a model of the hysteresis test configuration is presented.

Model of Logarithmic Decrement Test

The first model developed to verify test results is described by the equation

$$m\ddot{z} + c\dot{z} + 76{,}300(z)^{2.147} = mg \tag{5}$$

where m and c are the mass and viscous damping coefficient, respectively, and the functional form of the stiffness term was obtained by curve fitting the static stiffness data. For absolute displacement, the weight must be included on the right-hand side of the equation. It is noted that z is the displacement of the mass-loaded end of the TABI system shown in Fig. 7. The viscous damping coefficient c was estimated using the logarithmic decrement method, as discussed previously. For systems with damping less than about 20% of critical, the damping coefficient can be expressed approximately as

$$c = m\omega_n \ln (u_p/u_q)/\pi \tag{6}$$

where u_p and u_q are the amplitudes of vibration one cycle apart.

Numerical solutions of Eq. (5) initially showed poor agreement with the test data. The analytical natural frequency of the TABI/mass system was approximately 15 Hz, compared to 30 Hz for the physical system. The discrepancy was of such magnitude as to reveal a fundamental error in the model. It was discovered that the static stiffnesses are not representative of the dynamic stiffnesses for TABI and that analytical models must account for this observation. Dynamic magnification factors were calculated for two different tests by using the simple relation for natural frequency of a one-dimensional system, $\omega_n = \sqrt{k/m}$. Since the measured frequency was consistently near 30 Hz, even for different masses, and the mass loads were known, the corresponding dynamic stiffness could be computed. The average ratio of the calculated dynamic stiffness to measured static stiffness was 3.15 for the tests checked. It was also found that a constant magnification factor applied to an entire static stiffness curve adequately represented the measured response frequency and magnitude. In Fig. 15, static and dynamic stiffness curves are compared for a typical TABI sample of the type shown in Fig. 3. Solutions of Eq. (5) using dynamic restoring force expressions of the form

$$f(z) = 236{,}534(z)^{2.147} \tag{7}$$

yielded reasonable agreement with experiment. Further information on the investigation of TABI dynamic stiffness is provided in Ref. 11.

Model of Hysteresis Damping Test

Results of the hysteresis curve measurements were verified using a model similar to Eq. (5):

$$m\ddot{z} + c(\Omega,Z)\dot{z} + [k(z \pm \epsilon^2 z^3) + b] = F(t) \tag{8}$$

In this model, the damping coefficient changes depending on the frequency and amplitude of excitation, as can be seen from Figs. 12 and 13. The stiffness expression was again derived from a curve fit of the static stiffness data, and the dynamic magnification factor was used as discussed in the last section.

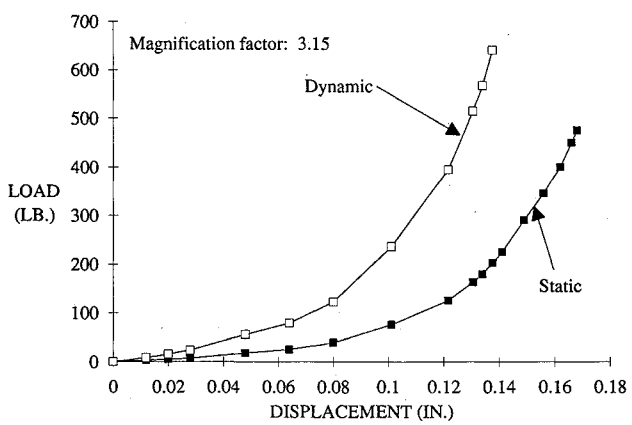

Fig. 15 Static and dynamic stiffness curves for typical TABI sample.

The functional form of the stiffness expression represents a general cubic variation in the restoring forces and has been used in modeling of flexible cable systems.[18] Both k and ϵ are variable, depending on the displacement z. The parameter b is the distance the hysteresis curve lies above the origin for zero displacement.

From the test data, the displacement at the lower edge of the TABI (Fig. 11) is known. Assuming harmonic motion and rewriting Eq. (8) with $F(t) = 0$,

$$-m\Omega^2 Z \sin \Omega t + c(\Omega,Z)\Omega Z \cos \Omega t + \{k[Z \sin \Omega t \pm \epsilon^2(Z \sin \Omega t)^3] + b\} = 0 \quad (9)$$

where Ω and Z are the frequency and amplitude of the excitation (or response), respectively. The force transmitted to the fixture at the upper edge of the material (Fig. 11) is the sum of the stiffness and damping terms,

$$F_{tr} = c(\Omega,Z)\Omega Z \cos \Omega t + \{k[Z \sin \Omega t \pm \epsilon^2(Z \sin \Omega t)^3] + b\} \quad (10)$$

and the analytical hysteresis curves are obtained by plotting this transmitted force vs the mass displacement or acceleration.

It is noted that, for practical application of Eq. (10), it was more convenient and accurate to obtain each k from the corresponding experimental hysteresis curve and to neglect ϵ. Taking this approach, numerical hysteresis curves were generated and compared to experiment, as shown in Figs. 16 and 17 for two cases. Again it appears that TABI in-plane damping can be modeled as a form of viscous damping for low amplitudes.

Further discussion of the relation between static and dynamic stiffnesses of TABI is in order at this point. It was stated previously in reference to Fig. 15 that a constant magnification factor applied to an entire static stiffness curve adequately represented the system response for the log decrement test. However, for modeling of the hysteresis test setup, it was found that the use of an average stiffness obtained from each experimental hysteresis curve gave better results than the modified static stiffness curve. This simply means that the dynamic stiffness curve shown in Fig. 15 has insufficient detail for very small displacements (below 0.02 in.). Dynamic stiffnesses obtained from hysteresis data should be used in general for that displacement range.

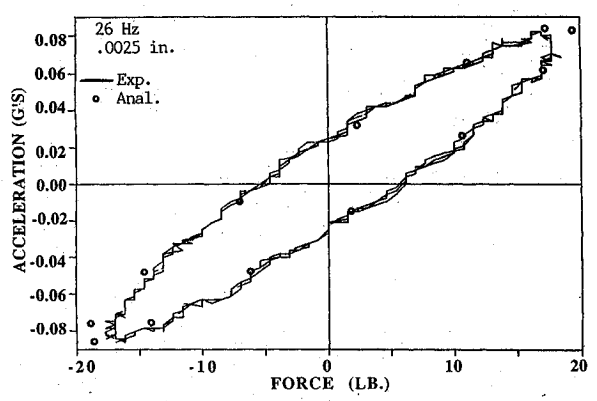

Fig. 16 Comparison of experimental and analytical hysteresis curves, 26 Hz.

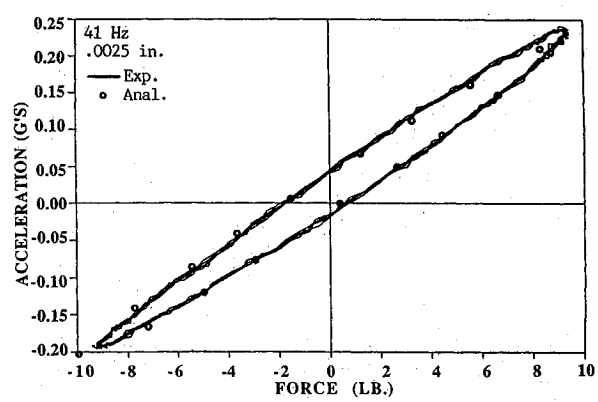

Fig. 17 Comparison of experimental and analytical hysteresis curves, 41 Hz.

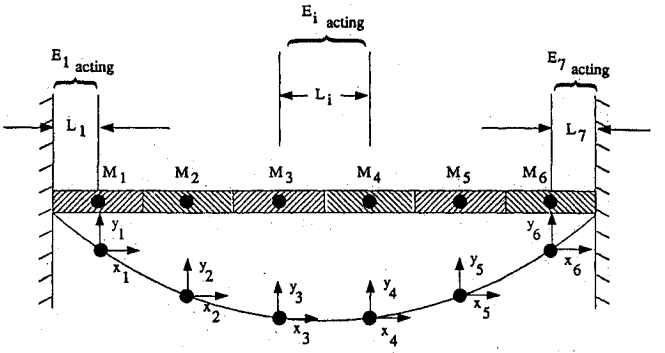

Fig. 18 Finite difference model of TABI system.

Transverse Properties of Tailorable Advanced Blanket Insulation

In an aerobraking application of TABI, it is expected that out-of-plane motion will be more significant than motion in the plane of the material. A major concern in this study was to determine if the in-plane material properties measured as described in a previous section are valid for the transverse degrees of freedom. The out-of-plane stiffnesses for a cloth structure are functions of the in-plane stress state. Without planar stresses (preload), the transverse stiffnesses are zero and numerical matrix solutions become singular. Therefore, initial conditions must be provided in finite element models to ensure a nonzero planar stress state. This provision corresponds to the requirement of tensile preloads in the damping tests described previously. In this section, a finite difference time domain model that does not rely on in-plane stress stiffening is utilized to investigate transverse behavior of TABI using in-plane stiffness and damping data.

Using the relationship that equates the distance between two points, along with trigonometric expressions for the angle between the points, a model of the TABI strip used in the experimental study was developed. The strip was divided into six segments of equal length with the mass lumped at the centers of the segments, as shown in Fig. 18. Damping was evenly distributed among the segments, and the damping coefficients used were those obtained in the log decrement tests. The equations of motion for each segment are given in Eqs. (11) and (12):

$$\frac{AE_{i+1}}{L_{i+1}}\left[\sqrt{(y_{i+1}-y_i)^2+(x_{i+1}-x_i)^2}-L_{i+1}\right] \times \cos\left[\tan^{-1}\left(\frac{y_{i+1}-y_i}{x_{i+1}-x_i}\right)\right] - \frac{AE_i}{L_i}\left[\sqrt{(y_i-y_{i-1})^2+(x_i-x_{i-1})^2}-L_i\right] \times \cos\left[\tan^{-1}\left(\frac{y_i-y_{i-1}}{x_i-x_{i-1}}\right)\right] + C\sqrt{(\dot{y}_{i+1}-\dot{y}_i)^2+(\dot{x}_{i+1}-\dot{x}_i)^2}\cos\left[\tan^{-1}\left(\frac{\dot{y}_{i+1}-\dot{y}_i}{\dot{x}_{i+1}-\dot{x}_i}\right)\right] - C\sqrt{(\dot{y}_i-\dot{y}_{i-1})^2+(\dot{x}_i-\dot{x}_{i-1})^2}\cos\left[\tan^{-1}\left(\frac{\dot{y}_i-\dot{y}_{i-1}}{\dot{x}_i-\dot{x}_{i-1}}\right)\right] = M_i\ddot{x}_i \quad (11)$$

$$\frac{AE_{i+1}}{L_{i+1}}\left[\sqrt{(y_{i+1}-y_i)^2+(x_{i+1}-x_i)^2}-L_{i+1}\right]\times\sin\left[\tan^{-1}\left(\frac{y_{i+1}-y_i}{x_{i+1}-x_i}\right)\right]-\frac{AE_i}{L_i}\left[\sqrt{(y_i-y_{i-1})^2+(x_i-x_{i-1})^2}-L_i\right]\times\sin\left[\tan^{-1}\left(\frac{y_i-y_{i-1}}{x_i-x_{i-1}}\right)\right]+C\sqrt{(\dot{y}_{i+1}-\dot{y}_i)^2+(\dot{x}_{i+1}-\dot{x}_i)^2}\sin\left[\tan^{-1}\left(\frac{\dot{y}_{i+1}-\dot{y}_i}{\dot{x}_{i+1}-\dot{x}_i}\right)\right]-C\sqrt{(\dot{y}_i-\dot{y}_{i-1})^2+(\dot{x}_i-\dot{x}_{i-1})^2}\sin\left[\tan^{-1}\left(\frac{\dot{y}_i-\dot{y}_{i-1}}{\dot{x}_i-\dot{x}_{i-1}}\right)\right]=M_i\ddot{y}_i \quad (12)$$

Each mass M_i is equal to one-sixth of the total mass of the TABI strip, and the moduli of elasticity are given by

$$E_i = E(\epsilon_i) = 1{,}845{,}200\left\{\frac{\left[\sqrt{(y_i-y_{i-1})^2+(x_i-x_{i-1})^2}-L_i\right]}{L_i}\right\}^{1.147} \quad (13)$$

where

$$\epsilon_i = \left[\sqrt{(y_i-y_{i-1})^2+(x_i-x_{i-1})^2}-L_i\right]/L_i \quad (14)$$

From comparison of Eqs. (13) and (1), it can be seen that E_i is the finite difference form of the empirical modulus expression for the fill direction.

In order to compare transverse and in-plane deflections of TABI using in-plane structural properties, the model described in Eqs. (11–13) and shown in Fig. 18 was solved numerically for the sudden vertical release of a 150-lb weight attached at the center of the TABI strip. The transverse response is shown in Fig. 19 and compared to the axial response computed using Eq. (5). The axial response corresponds to the logarithmic decrement test configuration (Fig. 7), where a 150-lb weight was released suddenly and the TABI/mass system was allowed to oscillate freely. It can be seen from Fig. 19 that the transverse stiffness is considerably lower than the in-plane stiffness, as expected. Therefore, the higher-amplitude, lower-frequency modes of TABI or any cloth structure will be dominant in the out-of-plane degrees of freedom.

The effect of in-plane prestressing of the TABI strip was also investigated using Eqs. (11–13). A 30-lb step function was applied to nodes 3 and 4 in the transverse direction, and the responses for no preload and a preload corresponding to a

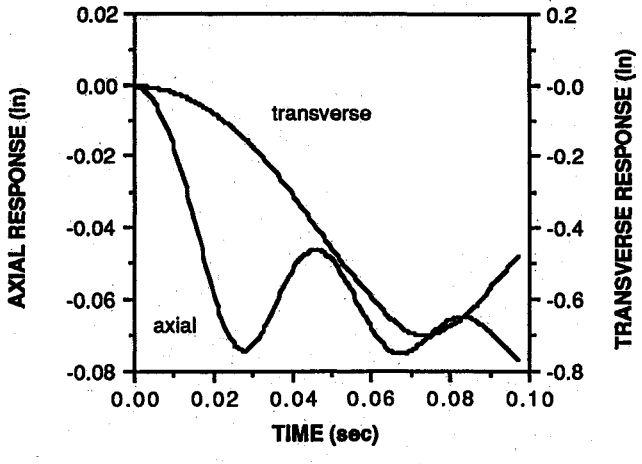

Fig. 19 Comparison of in-plane and transverse stiffnesses.

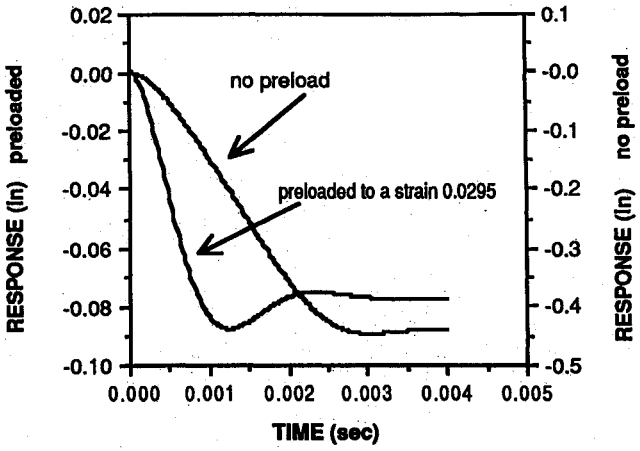

Fig. 20 Effect of in-plane preload on transverse TABI response.

0.0295 strain are compared in Fig. 20. The in-plane preload is seen to decrease the transverse deflection and to increase the response frequency. Both of these effects are reasonable and were expected.

Use of measured in-plane TABI properties for out-of-plane response prediction is shown to yield reasonable and expected behavior. Therefore, it is concluded that use of in-plane material properties is valid for calculation of transverse properties for TABI and flexible fabric structures in general.

Summary

In this study, the most significant material properties necessary for dynamic modeling of an advanced flexible TPS at room temperature have been obtained and verified in analytical models. It has been shown that TABI is a highly nonlinear material that stiffens as the load applied to it increases. Both the damping and stiffness characteristics of TABI are quite complex, varying as functions of both frequency and amplitude of excitation. Use of the in-plane material properties for calculation of transverse properties has been demonstrated and shown to yield reasonable results.

Acknowledgments

Damping tests for this study were conducted by the Dynamics Test Branch at Marshall Space Flight Center under the direction of A. D. Coleman. Special appreciation is expressed to Paul Dumbacher for his work in designing the hysteresis test configuration and developing graphics software for the tests.

References

[1]Sawko, P. M., "Tailorable Advanced Blanket Insulation (TABI)," NASA CP-3001, Nov. 1987, pp. 135–152.

[2]Tinker, M. L., "Deployable Aerobrake Structural Development," NASA TM-103510, Feb. 1990, pp. 199, 200.

[3]Sawko, P. M., "Flexible Thermal Protection Materials," NASA CP-2315, Dec. 1983, pp. 179–192.

[4]Kourtides, D. A., Pitts, W. C., Araujo, M., and Zimmerman, R. S., "High Temperature Properties of Ceramic Fibers and Insulation for Thermal Protection of Atmospheric Entry and Hypersonic Cruise Vehicles," *SAMPE Quarterly*, Vol. 19, No. 3, 1988, pp. 8–18.

[5]Calamito, D. P., "Development of Tailorable Advanced Blanket Insulation for Advanced Space Transportation Systems," NASA CR-177444, April 1987.

[6]Mui, D., and Clancy, H. M., "Development of a Protective Ceramic Coating for Shuttle Orbiter Advanced Flexible Reusable Surface Insulation (AFRSI)," *Ceramic Engineering and Science Proceedings*, Vol. 6, Nos. 7–8, 1985, pp. 793–805.

[7]Savage, R. T., Love, W., and Bloetscher, F., "High Temperature Performance of Flexible Thermal Protection Materials," AIAA Paper 84-1770, June 1984.

[8]Pusch, R. H., "Thermal Blanket Insulation for Advanced Space Transportation Systems," NASA CR-177341, Feb. 1985.

[9]Pitts, W. C., and Murbach, M. S., "Thermal Design of Aero-

assisted Orbital Transfer Vehicle Heat Shields for a Conical Drag Brake," *Journal of Spacecraft and Rockets,* Vol. 23, No. 4, 1986, pp. 442–448.

[10]Clayton, J. P., and Knox, E. C., "TABI Thermal and Structural Properties," Remtech, Inc., RTR 195-1-01, Huntsville, AL, Dec. 1988.

[11]Clayton, J. P., "TABI Mechanical Properties, Test Results and Subsystem Test Design," Remtech, Inc., RTR-195-1-03, Huntsville, AL, Oct. 1989.

[12]Bobinger, D. A., "Non-Linear Analysis of Axisymmetric Rubber Structures," AIAA Paper 83-0902, May 1983.

[13]Harris, C. M., and Crede, C. E. (eds.), *Shock and Vibration Handbook,* 2nd ed., McGraw-Hill, New York, 1976, pp. 35-8–35-12, 37-7–37-9.

[14]Belvin, W. K., and Edighoffer, H. H., "15 Meter Hoop-Column Antenna Dynamics: Test and Analysis," NASA CP-2447, Nov. 1986, pp. 167–185.

[15]Craig, R. R., Jr., *Structural Dynamics: An Introduction to Computer Methods,* Wiley, New York, 1981, p. 59.

[16]Steidel, R. F., Jr., *An Introduction to Mechanical Vibrations,* 3rd ed., Wiley, New York, 1989, pp. 189–191.

[17]Dahl, S. R., and Rice, R. B., "A Derivation of Equivalent Linear Viscous and Elastic Constants for Viscoelastic Materials," Air Force Wright Aeronautical Labs., AFWAL-TR-84-3064, Wright-Patterson AFB, OH, Feb. 1984, pp. O-1–O-9.

[18]Tinker, M. L., and Cutchins, M. A., "Damping Phenomena in a Wire Rope Vibration Isolation System," *Proceedings of 1st International Congress on Air- and Structure-Borne Sound and Vibration,* Auburn Univ., Auburn, AL, March 1990, pp. 405–412.

Earl A. Thornton
Associate Editor